Disappearance of dimits shift in realistic fusion reactor plasmas with negative magnetic shear

Dingkun Yang[1,3], **Shengming Li**[1,4], **Yong Xiao**[1,*] and **Zhihong Lin**[2]

[1] Institute for Fusion Theory and Simulation, School of Physics, Zhejiang University, Hangzhou 310027, China
[2] Physics and Astronomy, UC Irvine, Irvine, CA 92697, United States of America

E-mail: yxiao@zju.edu.cn

CrossMark

Abstract

This study employs gyrokinetic simulations to investigate ion temperature gradient (ITG) turbulence in realistic fusion reactor plasmas featuring reversed magnetic shear. The weakly negative magnetic shear is observed to be more stable for the ITG instability than strongly positive shear in this equilibrium configuration, primarily stemming from the scarcity of mode rational surfaces induced by the weak negative shear. This superiority in suppression for the negative shear persists in nonlinear turbulence with zonal flow artificially eliminated, where the emergence of turbulence solitons is observed and found associated with locally dense mode rational surfaces. However, the difference in transport levels among different magnetic shears diminishes in the presence of self-consistently generated zonal flow, accompanied by the disappearance of turbulence solitons. The nonlinear generation of zonal flow is found to be significantly affected by the magnetic shear. The study reveals a remarkable phenomenon that the Dimits shift no longer exists for negative magnetic shear, which is attributed to the weakness of the zonal flow generation near the ITG marginal stability.

Keywords: tokamak turbulent transport, drift wave, gyrokinetic simulation, dimits shift, zonal flow, magnetic shear

1. Introduction

Turbulent transport driven by drift wave instabilities is widely observed in fusion plasmas [1]. One of the common causes of ion turbulent transport in tokamaks is the Ion Temperature Gradient (ITG) instability [2–4], which significantly reduces the efficiency of fusion reactors. The profile stiffness propels fusion plasmas toward marginal stability [5, 6], resulting in the plasma temperature being determined by the critical temperature gradient. Consequently, even a slight elevation of the critical temperature could yield a remarkable increase in fusion power. While profile stiffness is widely observed, there exist a few exceptions including a recently discovered operational regime from the KSTAR tokamak [7], the FIRE mode, where the plasmas can be operated well above the critical temperature gradient.

The axisymmetric $E \times B$ rotation or zonal flow, self-consistently generated by turbulence, is generally accepted as a regulator of the saturation level of turbulent transport in fusion plasmas [8–13]. Near marginal stability, the zonal flow has been observed to completely suppress turbulence and transport, causing a nonlinear up-shift of the critical temperature gradient for ITG, known as the Dimits shift

---

[14, 15]. Although the zonal flow can be damped significantly by collisions [16, 17], the Dimits shift is found to exist not only in collisionless plasma but also in collisional plasma [18]. Due to its significance in understanding crucial dynamics in fusion plasmas, such as zonal flow-turbulence interaction and L-H transition [12, 19, 20], the physics mechanism about the Dimits shift is still under active investigation [21, 22].

Magnetic shear is another crucial factor that can regulate turbulence in fusion plasmas. Experimental and simulation analyses have shown that reversed magnetic shear significantly affects particle and heat transport in toroidal plasmas through suppressing linear instabilities [23, 24]. A promising ITER operation scenario called advanced operation mode is characterized by weak reversed magnetic shear and non-inductive current drive [25]. The interplay among magnetic shear, linear instability, zonal flow, and turbulent transport in this scenario remains not fully understood, particularly regarding the potential impact of magnetic shear on the nonlinear generation of zonal flow and subsequent turbulent transport.

In this study, our findings show that negative (reversed) shear has the ability to suppress linear ITG instability, which is due to the scarcity of mode rational surfaces induced by the weak negative magnetic shear. However, nonlinear turbulent transport does not align with the trend observed in linear instability. Instead, it converges to the same transport level irrespective of the magnetic shear when the plasma is away from marginal stability and a self-consistent zonal flow is generated. On the contrary, in the absence of a self-consistently generated zonal flow, nonlinear transport aligns with the trend of linear instability. Additionally, our study reveals that the presence of zonal flow alters the pattern of turbulence propagation by eliminating turbulent solitons induced by the local high density of mode rational surfaces. Moreover, the nonlinear generation of zonal flow is found to be significantly influenced by the magnetic shear. A noteworthy observation is the disappearance of the widely observed Dimits shift under negative magnetic shear. Our study further uncovers that negative magnetic shear results in a weaker zonal flow, consequently diminishing the linear suppression effect and causing the Dimits shift to vanish. This observation underscores the crucial role of magnetic shear in regulating turbulent transport through the mediation of zonal flow, thereby exerting a broad impact on global turbulent transport in advanced tokamak operation modes.

2. Simulation parameters

In this letter, we conduct electrostatic global gyrokinetic simulations [26–28] in the collisionless limit using the Gyrokinetic Toroidal Code (GTC) to investigate the influence of magnetic shear on ITG turbulence and transport, focusing on interactions between turbulence, magnetic shear and zonal flow relevant to reactor-size fusion plasmas. The equilibrium magnetic field used in the simulations is obtained from the design of the China Fusion Engineering Test Reactor (CFETR) [29, 30], which features strong shaping and reversed

magnetic shear, as depicted in figure 1. To simulate strongly shaped plasmas, we implement the modified four-point average method within the GTC code [31, 32]. For our simulations, we select three reference magnetic surfaces at the centers of the simulation domains, denoted as A, B, and C in figure 1(*a*), representing negative, zero, and positive magnetic shear, respectively.

The simulations employ the following major parameters: magnetic field at the magnetic axis $B_0 = 6.50\,\text{T}$, major radius $R_0 = 6.60\,\text{m}$, inverse aspect ratio $a/R_0 = 0.22$, on-axis electron density $n_0 = 7.80 \times 10^{19}\,\text{m}^{-3}$, $n_{i0} = n_0$ due to quasi-neutrality. Deuterium ions are used with a mass of $m_{\text{D}} = 2m_H = 3674m_e$. The on-axis temperature for both electrons and ions is $T_{\text{e0}} = T_{\text{i0}} = 13.00\,\text{keV}$, and the normalized minor radius a is approximately equal to $569\rho_i$. Here, the ion gyroradius ρ_i is calculated as $\rho_i = C_s/\Omega_i$, where $C_s = \sqrt{T_{\text{e0}}/m_{\text{D}}}$ and Ω_i represents the deuterium cyclotron frequency.

Figure 1(*b*) illustrates the poloidal cross-section of a typical CFETR equilibrium B field, depicting a strongly shaped plasma with elongation $\kappa = 2.1$ and triangularity $\delta = 0.1$ at $r = 0.5a$. The central flux surfaces for different simulation domains are demonstrated by blue dashed lines for negative magnetic shear, red dash-dotted lines for zero magnetic shear, and black solid lines for positive magnetic shear. Each simulation domain spans 20% of the minor radius a, with $\Delta r \approx 100\rho_i$. The poloidal simulation domain for zero magnetic shear is denoted by the purple shaded area. We set the simulation grids with $\Delta r = 0.81\rho_i$ and $r\Delta\theta = 0.85\rho_i$. The simulation time step size is $\Delta t = 0.10R_0/C_s$, where $C_s/R_0 = 1.19 \times 10^5\,\text{s}^{-1}$. With these settings, the simulation precision is limited by gyro-average, i.e. $k_\theta\rho_i \leq 2.0$. In the nonlinear simulation, all toroidal modes that are numerically allowed are included. Consequently, the maximum permissible toroidal mode number is approximately $n \simeq 350$.

3. Linear simulation

Here we assume adiabatic electrons in the simulations to elucidate the essential physics since grand computational challenges are posed by the large size of the CFETR reactor. We focus on this strongly shaped plasma and begin by investigating the linear ITG dispersion relation while varying poloidal wavelength $k_\theta\rho_i$, and comparing the resulting linear growth rates and real frequencies for three different magnetic shears, as shown in figure 1. The strong plasma shaping featured by the CFETR design, is found to significantly enhance the threshold of the ITG instability, consistent with previous simulations [33, 34]. To excite the ITG instability, we set the temperature gradients much larger than those in the Cyclone Base Case (CBC), with $R/L_{Ti} = R/L_{Te} = 13.32$ and $R/L_n = 2.22$ for the present study. To facilitate linear simulation, the temperature and density profiles are configured as illustrated in figure 2, featuring flat gradient profiles centering around corresponding reference flux surface for each magnetic shear. Figure 3(*a*) shows the ITG growth rate as a function of $k_\theta\rho_i$ for negative magnetic shear (blue square line), zero
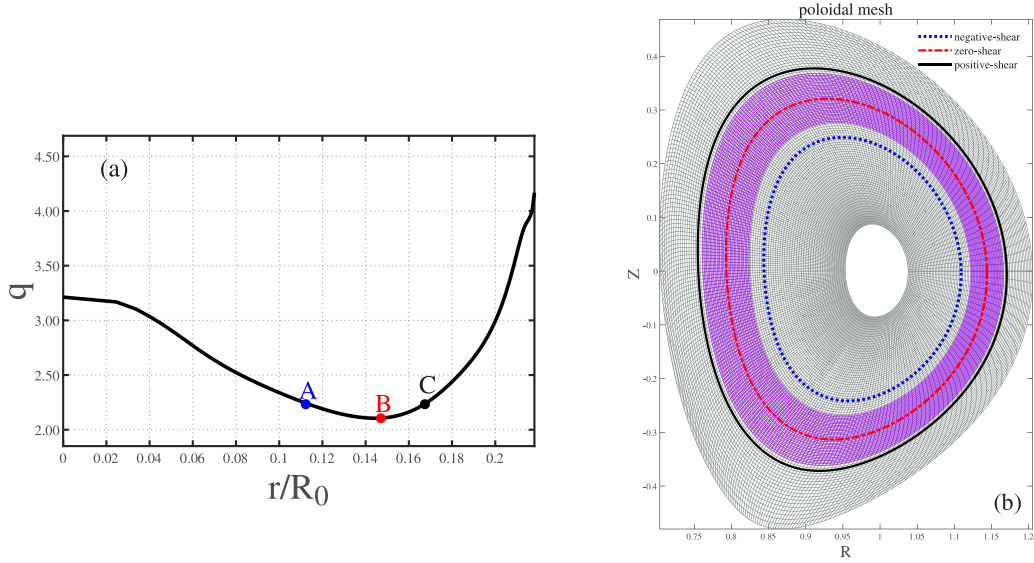
Figure 1. (*a*) Selection of three radial points as simulation domain centers: point A features negative magnetic shear, point B represents zero magnetic shear, and point C demonstrates positive magnetic shear. (*b*) Central flux surfaces within simulation domains centered around these three distinct magnetic shears.
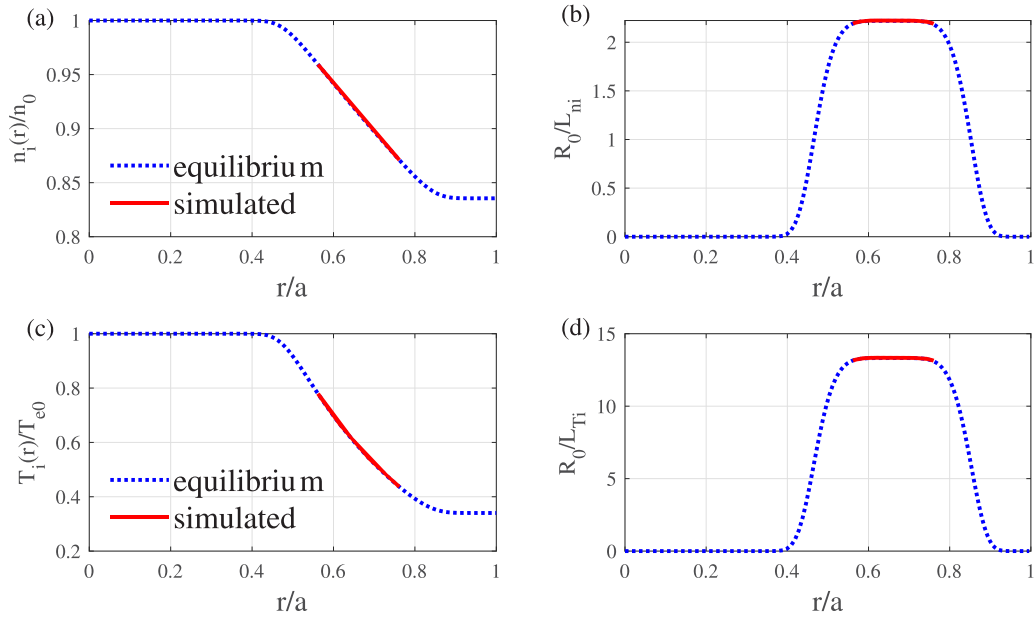

Figure 2. Radial density and temperature profiles, along with their respective gradients, employed in the simulation. The solid red line represents the simulation domain centered at point B in figure 1(*b*).

magnetic shear (red circle line), and positive magnetic shear (black triangle line) defined at reference points A, B, and C in figure 1, respectively. The linear growth rate significantly decreases as the magnetic shear changes from positive to negative, indicating the stronger stabilizing effect of the negative shear compared to the positive shear. This result is consistent with previous gyrokinetic simulations using CBC parameters with circular magnetic flux surfaces [23]. The maximum growth rate for positive magnetic shear is $\gamma = 0.15C_s/L_n$. The wavelength that maximizes the linear growth rate $k_\theta^{\max}$ is around $k_\theta^{\max}\rho_i = 0.78$, determined by the effective perpendicular wavelength $k_\theta^{\mathrm{eff}}\rho_i$, since the effective poloidal wavelength

$k_\theta^{\mathrm{eff}}\rho_i = \frac{k_\theta\rho_i}{\kappa} = 0.37$ [33], which is consistent with the CBC case [35].

Subsequently, we examine the dependence of the maximum linear growth rate $\gamma_{\max}$ on the ITG or $\eta_i \equiv \frac{\mathrm{d}\ln T_i}{\mathrm{d}\ln n_i}$ for the ITG instability, presented in figure 3(*b*) for $R/L_n = 2.22$ and $k_\theta\rho_i = 0.78$. We observe that $\gamma_{\max}$ increases almost linearly with η_i, with the same slope for different magnetic shears, suggesting that magnetic shear is decoupled from η_i in determining $\gamma_{\max}$. Additionally, the linear simulation results suggest that the real frequency $\omega_r \propto \omega_{*i}(1 + \eta_i)$, where ω_{*i} is the ion diamagnetic frequency, consistent with theoretical predictions. These linear simulations confirm the reliability of the
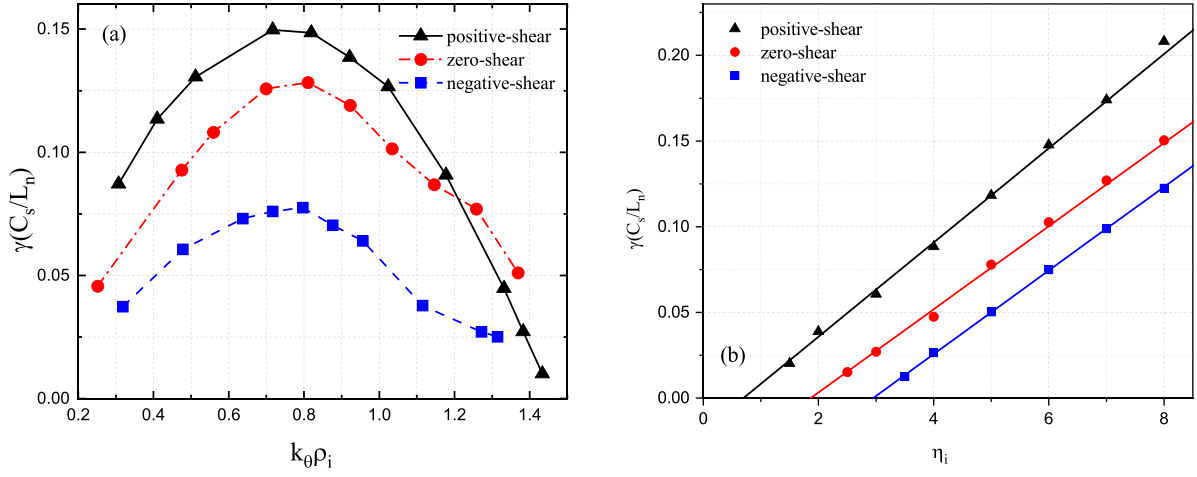
Figure 3. Variation of linear growth rate as a function of wavelength $k_\theta \rho_i$ (*a*) and ion temperature gradient or η_i (*b*) for the ITG instability (adiabatic electrons) under different magnetic shear conditions.
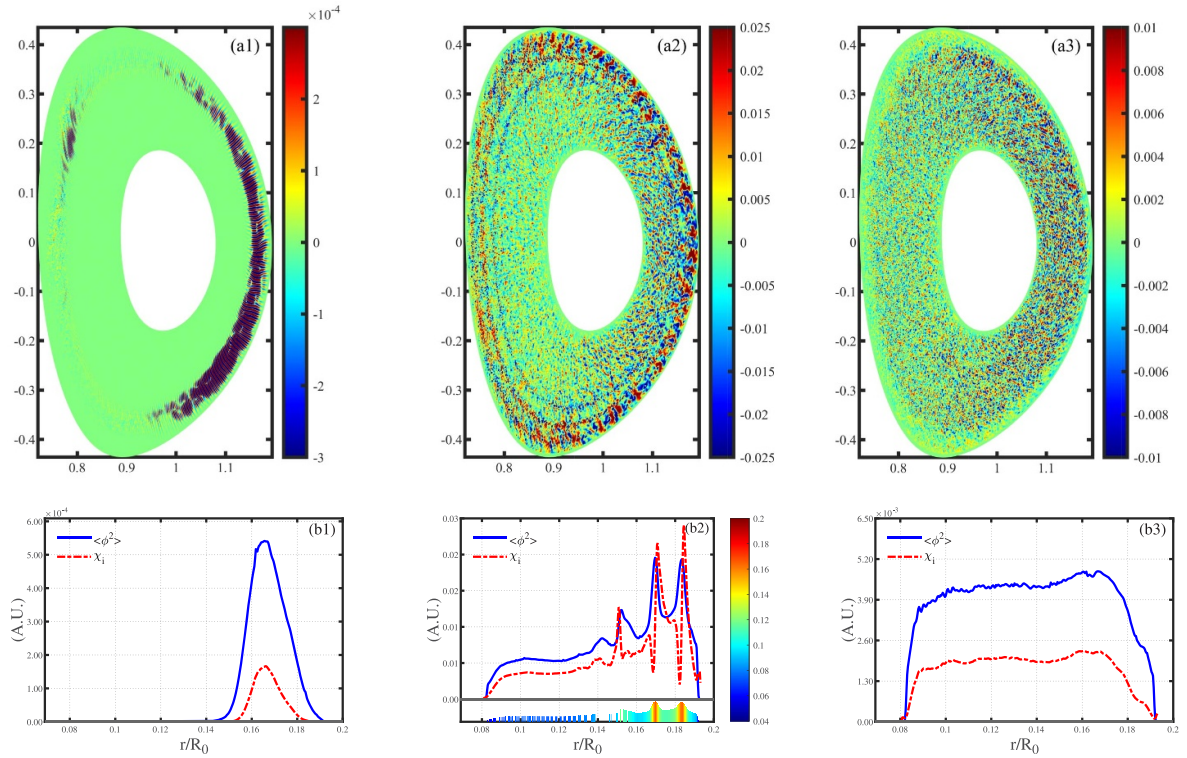

Figure 4. (*a*1–*a*3) - Poloidal turbulence contour of lTG mode under reversed magnetic shear: (*a*1) - linear stage, (*a*2) - nonlinear stage without zonal flow, (*a*3) - nonlinear stage with zonal flow. (*b*1–*b*3) - Radial profiles of ion heat conductivity (red dashed line) and turbulence intensity (blue solid line) after flux surface and time averaging: (*b*1) - linear stage, (*b*2) - nonlinear stage without zonal flow, with the lowest part showing the mode rational surface density weighted by growth rate, (*b*3) - nonlinear stage with zonal flow.

GTC code in simulating the ITG mode for realistic strongly shaped tokamak plasmas.

We proceed by expanding the simulation domain to encompass the entire reversed magnetic shear profile with $\eta_i = 6.0$, conducting nonlinear ITG simulations within this extended radial domain. Figure 4 displays the 2D poloidal electrostatic potential for reversed magnetic shear, with the self-consistent zonal flow retained in the right column (*a*3) and artificially removed zonal flow in the middle column (*a*2). The linear

mode structure is shown in the left column (*a*1). The second row presents the flux-surface-averaged turbulence intensity and ion heat conductivity for each case, indicating that ion heat transport is driven by local turbulent intensity. The physical quantities in figures 4(*b*2) and (*b*3) are time-averaged in the nonlinear saturation stage with a time window of $70R_0/C_s$. In the linear stage, the stronger stabilizing effect of negative shear on the linear instability confines the linear mode structure to the positive shear region. However, during the nonlinear

stage, potential fluctuations spread from the positive magnetic shear region to the negative magnetic shear region, as does ion heat transport. In the absence of self-consistent zonal flow, the radial turbulence structure exhibits bursty peaks corresponding to soliton structures previously observed in research [36]. Plotting the mode rational surface density weighted by the growth rate in figure 4(*b*2), we find that the radial positions of these turbulent solitons align with local maxima of the mode rational density profile, which implies that the turbulence solitons arise from concentration of mode rational surfaces and reinforcement of multiple toroidal modes. However, during the nonlinear stage, potential fluctuations spread from the positive magnetic shear region to the negative magnetic shear region [23, 37] , as does ion heat transport. In the absence of self-consistent zonal flow, the radial turbulence structure exhibits bursty peaks, which is shown by the blue line in figure 4(*b*2) and may correspond to the soliton structures previously observed in a slab geometry plasma [36]. These soliton structures give rise to a large amount of ion heat transport, as shown by the red line in figure 4(*b*2). Next we plot the mode rational surface density weighted by the growth rate, which shows a number of local maxima indicated by the red bulges above the lowest horizontal axis in figure 4(*b*2). Then we find that the radial positions of these turbulent solitons align with these local maxima, which implies that the turbulence solitons arise from the local concentration of mode rational surfaces and reinforcement of multiple toroidal modes. In contrast, when zonal flow is self-consistently excited, the radial distribution of both turbulence intensity and ion heat transport becomes much more uniform radially. This suggests that zonal flow can absorb strong local turbulence energy from densely packed mode rational surfaces, effectively eliminating the soliton structures in the ITG turbulence. Another possibility is that zonal flow propagation can expedite turbulence spreading and radial redistribution of turbulent energy.

4. Nonlinear simulation

Typical time histories of volume-averaged ion thermal conductivity, χ_i, are illustrated in figure 5 for different magnetic shears. Specifically, figure 5(*a*) corresponds to marginally unstable cases , while figure 5(*b*) depicts well-unstable cases with $\eta_i = 8.0$. As shown in figure 5(*a*), in the negative shear scenario, turbulent transport remains consistent for both cases with and without zonal flow, given identical $\eta_i = 3.5$. However, in the positive shear scenario, to achieve a comparable weak transport level, η_i needs to be 1.5 for the without-zonal-flow case and 3.0 for the with-zonal-flow case. These observations strongly imply a notable Dimits shift in the presence of positive shear but not in negative shear. From figure 5(*b*), it is evident that the saturation level remains nearly unchanged despite varying magnetic shears, irrespective of their distinct linear growth rates. We further note that the continuous decrease in heat flux towards the end of the simulation is a widespread phenomenon in global gyrokinetic simulations, usually attributed to profile relaxation in the global gyrokinetic simulation [38].

Next, we perform a time-averaging of the ion thermal conductivity during the nonlinear saturation stage for different magnetic shears within the shaded regions illustrated in figure 1(*b*). The resulting saturated χ_i is then plotted as a function of the ITG, η_i, while keeping the density gradient fixed, as shown in figure 6. In this plot, the shaped markers represent data from the GTC simulation, while the continuous lines are obtained through numerical curve fitting to illustrate the overall trend.

It is evident that, in the absence of zonal flow, the ion thermal conductivity χ_i increases rapidly with η_i. However, when self-consistent zonal flow is generated, χ_i increases at a much slower rate with η_i and eventually reaches a plateau value, regardless of the magnetic shear, as is demonstrated in figure 6. This suggests that the zonal flow serves as the dominant saturation mechanism, significantly reducing χ_i. Nevertheless, this regulatory effect of the zonal flow weakens for the negative magnetic shear case near the marginal stability point. This can be seen by comparing the critical temperature gradient or η_{ic} in figure 6.

As η_i decreases to a critical value η_{ic}, ion heat diffusivity χ_i becomes negligibly small due to the weak instability drive and turbulence. We then can calculate η_{ic} values for various magnetic shears, considering both cases with and without zonal flow, as presented in table 1. The phenomenon of the nonlinear upshift for the critical η_i, also known as the Dimits shift, is a well-established piece of nonlinear physics attributed to the zonal flow [15]. Analysis of table 1 reveals that the Dimits shift diminishes under negative magnetic shear, whereas it persists for positive magnetic shear scenarios. Additionally, it is worth noting that η_{ic} extracted from the case without zonal flow (see figure 6) aligns with the trend observed in the linear growth rate analysis for the negative shear case (refer to figure 3(*b*)). However, for the positive shear case, the η_{ic} derived from the linear growth rate trend is 0.8, which is lower than the nonlinear value of 1.46 obtained from figure 6. This discrepancy may stem from the nonlinear transport ceasing to grow earlier than anticipated by linear growth due to profile relaxation in the global simulation, indicating proximity to marginal stability.

A study reported previously that for the reversed shear case, turbulent transport does not decrease compared to the positive shear case due to turbulence spreading from positive shear regions to negative regions [23]. However, when away from marginal stability, the turbulent transport for the negative magnetic shear case resembles that of the positive shear case, which cannot be easily explained by the turbulence spreading picture [23]. In this well unstable regime, although the instability drive becomes stronger, the zonal flow generation is also stronger and in turn provide a stronger regulation effect. This suggests that the turbulent transport reaches some fixed point in the strong drive limit, as depicted in the predator-prey turbulence-zonal model [12], which requires further theoretical investigation.

The time-radial structure of zonal flow is shown in figures 7(*a*)–(*c*). It is shown that close to the marginal stability, the zonal flow has a relative global structure and can hardly propagate in the radial direction. However, away from the marginal stability, finer structure zonal flow is excited by
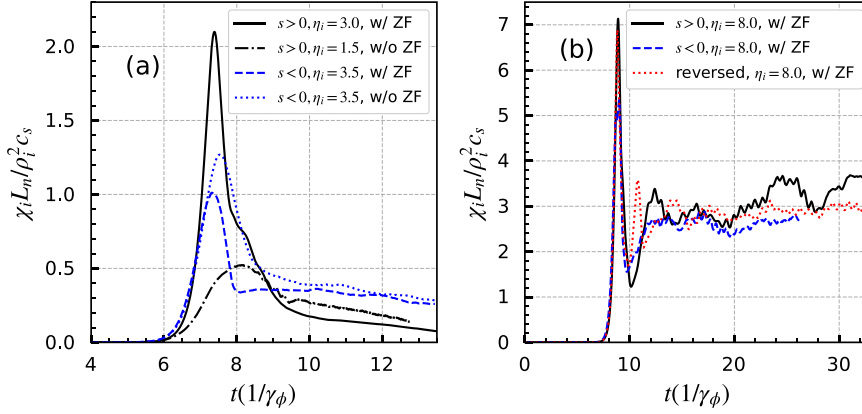
Figure 5. Time history of ion thermal conductivity χ_i for various magnetic shears (*a*) marginally unstable; (*b*) well unstable: $\eta_i = 8.0$.

Table 1. Critical η_i for ITG turbulence caused by the presence or absence of zonal flows for various magnetic shears.

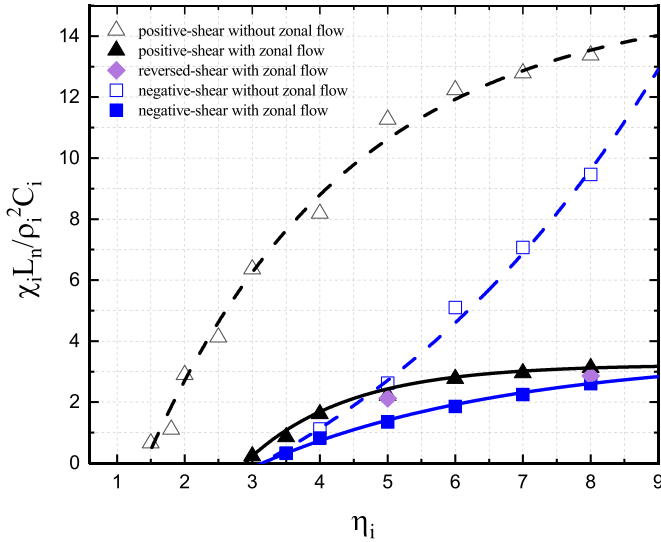| Shear	Negative	Positive
w/0 zonal	3.23	1.46
With zonal	3.25	2.88
NL upshift	0.02	1.42

Figure 6. Ion thermal conductivity, χ_i, varies with η_i for various magnetic shears with or without zonal flow.

turbulence and start propagating in the radial direction. The detailed radial mode structure of zonal flow for typical magnetic shears and η_i values is shown in figure 7(*d*). In the regime close to marginal stability, when $s > 0$, there is a strong long wavelength zonal flow left which can help suppress the turbulence and leads to the Dimits shift; when $s < 0$, the long-wavelength zonal flow cannot be easily excited, which implies the existence of modulational instability [39].

The intriguing observation of the vanishing Dimits shift under negative magnetic shear merits further investigation, as the underlying physics mechanism responsible for the Dimits shift lies in the essential nonlinear interaction between turbulence and zonal flow. To shed more light on this fascinating aspect of physics, we closely examine the nonlinear saturation of zonal flow during the initial stage of a multi-n mode simulation. As illustrated in figure 6, the saturated zonal flow and turbulence potential are represented as a function of the instability drive η_i. As the ITG mode approaches marginal stability, the magnitude of the drift wave diminishes, reaching a transport-insignificant level regardless of the magnetic shear. For the negative shear case, the zonal flow magnitude also approaches a level similar to that of the drift wave. However, in the positive shear case, the zonal flow magnitude reaches a much higher level. It is the disparity between the drift wave and the zonal flow around marginal stability that governs the significance of the Dimits shift. This observation may hold the key to gaining crucial insights into revisiting the theory of zonal flow-turbulence interaction. A thorough understanding the vanishing of Dimits shift under negative shear requires further theoretical and simulation efforts.

The limited generation of zonal flow for the negative shear case may be attributed to the plasma shaping effect on the residual zonal flow level. To assess the impact of magnetic geometry, we calculate the Rosenbluth–Hinton residual zonal flow level [9] using the GTC code at $k_\theta \rho_i = 0.14$ for the three reference points depicted in figure 1(*a*). The numerical results for residual zonal flow align with the analytic theory [40], as illustrated in figure 9. Notably, the residual zonal flow at the negative magnetic shear point is 30% lower than that at the positive magnetic shear point. However, this discrepancy cannot fully explain the 100% difference in zonal flow levels observed in the nonlinear ITG simulation near marginal stability, as shown in figure 8.

To further investigate the geometry effects, we conducted several control ITG simulations under negative and positive magnetic shears with circular cross-section plasmas, as shown in figure 10. Remarkably, the disappearance of the Dimits shift persists even when eliminating the plasma shaping effect. However, when a positive magnetic is prescribed, the Dimits shift comes back again. Consequently, we may conclude that the vanishing of the Dimits shift is primarily dependent on magnetic shear rather than equilibrium magnetic geometry.
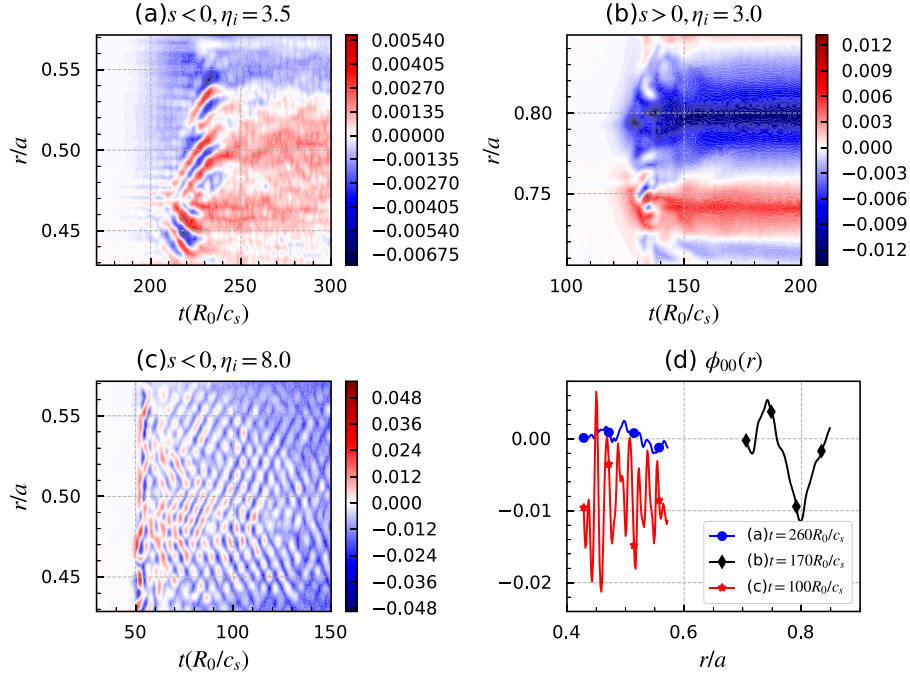
Figure 7. (*a*)–(*c*) Time-radial 2D structure of zonal flow for different magnetic shears and η_i values. (*d*) Radial zonal flow structure in the turbulence saturation stage.
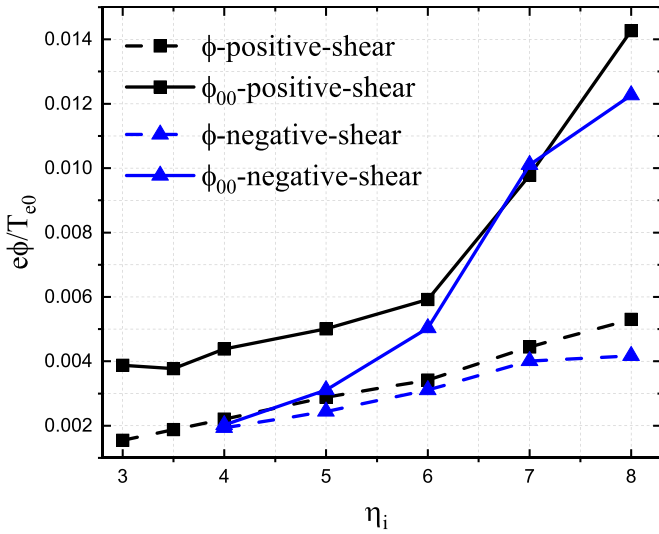

Figure 8. Saturation levels of zonal flow and ITG turbulence across different η_i values.

Figure 9. Residual zonal flow with CFETR equilibrium magnetic field from analytic theory and numerical simulation.

To distinguish the impact of geometric effects and magnetic shear on the Dimits shift, we make a comprehensive list of known cases from the literature as well as the simulation results of this paper, as shown in table 2. Utilizing parameters such as the safety factor q, inverse aspect ratio $\epsilon = r/R_0$, and shaping factors [40], we calculate the Rosenbluth–Hinton residual zonal flow R_{ZF}, as presented in table 2. The data in this table inevitably suggests that the disappearance of the Dimits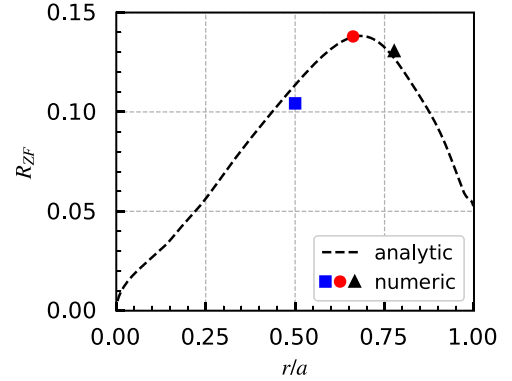 shift is more closely associated with negative magnetic shear rather than the residual zonal flow level. For example, the negative-shear CFETR case presented in this paper, has a larger residual zonal flow level than circular cross-section case with positive shear shown in figure 10(*a*). However, in the negative-shear CFETR case, no Dimits shift occurs, contrasting with the significant Dimits shift observed in the positive-shear circular cross-section case. Remarkably, when the magnetic shear is changed to negative in the circular cross-section case, the Dimits shift vanishes accordingly. These findings collectively suggest that the disappearance of the Dimits shift correlates strongly with negative magnetic shear rather than with plasma shaping or residual zonal flow level.
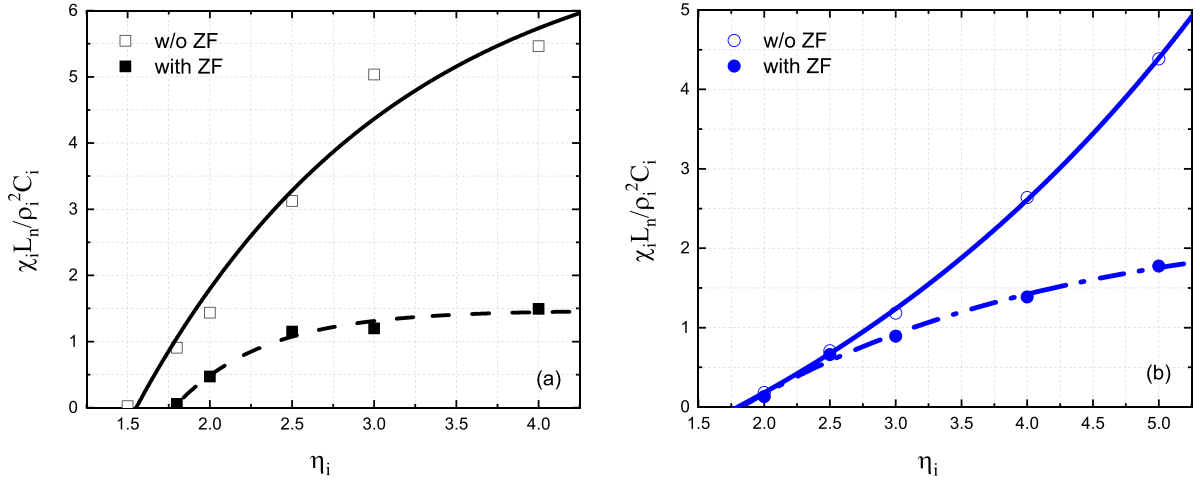
Figure 10. Ion thermal conductivity χ_i varies with temperature gradient or η_i for circular cross-section tokamak plasmas, where $a/R_0 = 0.36$, $R/L_{ni} = 2.2$: (*a*) positive magnetic shear $s = 0.78$; (*b*) negative magnetic shear $s = -0.36$.

Table 2. Residual zonal flow and Dimits shift.

Case	q	ε	shaping	R_{ZF}	$\hat{s}$	Dimits shift
Dimits2000 [15]	1.4	0.18	No	0.119	0.776–0.796	Yes
Rogers2000 [21]	1.4	0.167	No	0.115	0.8	Yes
Mikkelsen2008 [18]	1.3	0.179	Yes	0.227	1.16	Yes
CFETR(this paper)	2.27	0.109	Yes	0.104	−0.36	No
Circular(this paper)	2.38	0.182	No	0.045	−0.36	No
Circular(this paper)	2.38	0.182	No	0.045	0.78	Yes

5. Summary and conclusion

In summary, we have investigated the nonlinear interactions between linear ITG instability, zonal flow and magnetic shear for the ITG turbulence in strongly shaped fusion plasmas featuring weak reversed magnetic shear, as well as their consequences on transport. By comparing ITG instabilities under different magnetic shears, we found that the weak negative magnetic shear can suppress ITG instability more effectively by inducing scarce distribution for mode rational surfaces. This superiority in suppression for (weaker) negative shear persists even in the nonlinear ITG turbulence with the zonal flow artificially removed, where the appearance of turbulent solitary structures is consistent with the local concentration of the mode rational surfaces. However, in cases away from marginal stability and with self-consistent generation of zonal flows, the turbulent transport is primarily regulated by the zonal flows regardless of the magnetic shears, accompanied by the disappearance of turbulent solitary structures. We further investigated the magnetic shear effect on the generation of zonal flow and observed a remarkable physical phenomenon: under negative magnetic shear, the widely observed Dimits shift disappears. As tokamaks are prone to operate near marginal stability owing to profile stiffness, the Dimits shift proves to be practically useful by easing the edge temperature requirement. The potential loss of the Dimits shift in weak negative shear conditions may hinder the realization of this advantage.

However, tor weak reversed magnetic shear in the advance operational scenarios, the Dimits shift remain robust as our simulation results demonstrate. The vanishing of the Dimits shift is discovered due to the weakening of zonal flows by the negative magnetic shear near the marginal stability. While the disappearance of the Dimits shift under negative shear proves to be robust across various equilibrium magnetic geometries, such as circular cross-section or shaped plasmas, We acknowledge that the present study does not rule out the possibility of a transition between zero shear and negative shear. In a subsequent investigation, we will explore more about quantitative aspects of the Dimits shift transition from positive to negative shear.

In the last, we admit that there are some caveats about the current work. Although the simulations are carried out by global gyrokinetic code GTC, we try to limit the simulation setting in the local flux-tube region in order to isolate different magnetic shear effects, i.e. the simulations were conducted with flat gradient profiles. This kind of local setting naturally satisfies the conventional Dimit shift study using local code. However, for a real global simulation, the scenarios can get more complicated. According to the previous global gyrokinetic simulation study [37], the turbulence can spread from more strongly unstable region, into more stable region. If this stable region is caused by the Dimits shift, then one can still observe a fair amount of transport due to the turbulence spreading globally from the strongly

unstable region. Related to this, we clearly demonstrated in this CFETR reversed shear simulation, that the turbulence spreads from the positive shear region to the negative shear region, which is consistent with a previous study [41]. It requires further study whether Dimits shift is still robust when the nonlocal physics related to the radial variation of profile is strong.

Acknowledgments

ORCID iDs

Yong Xiao ⬤ https://orcid.org/0000-0001-5333-2867
Zhihong Lin ⬤ https://orcid.org/0000-0003-2007-8983

References

[1] Horton W. 1999 Drift waves and transport *Rev. Mod. Phys.* **71** 735
[2] Coppi B., Rosenbluth M. and Sagdeev R. 1967 Instabilities due to temperature gradients in complex magnetic field configurations *Phys. Fluids* **10** 582
[3] Romanelli F. 1989 Ion temperature-gradient-driven modes and anomalous ion transport in tokamaks *Phys. Fluids* B **1** 1018
[4] Dong J., Horton W. and Kim J. 1992 Toroidal kinetic η i-mode study in high-temperature plasmas *Phys. Fluids* B **4** 1867
[5] Doyle E. *et al* 2007 Plasma confinement and transport *Nucl. Fusion* **47** S18
[6] Horton W. 2012 *Turbulent Transport in Magnetized Plasmas* (World Scientific)
[7] Han H. *et al* 2022 A sustained high-temperature fusion plasma regime facilitated by fast ions *Nature* **609** 269
[8] Lin Z., Hahm T.S., Lee W., Tang W.M. and White R.B. 1998 Turbulent transport reduction by zonal flows: massively parallel simulations *Science* **281** 1835
[9] Rosenbluth M. and Hinton F. 1998 Poloidal flow driven by ion-temperature-gradient turbulence in tokamaks *Phys. Rev. Lett.* **80** 724
[10] Zonca F., Lin Y. and Chen L. 2015 Spontaneous excitation of convective cells by kinetic alfvén waves *Europhys. Lett.* **112** 65001
[11] Hahm T.S. 1994 Rotation shear induced fluctuation decorrelation in a toroidal plasma *Phys. Plasmas* **1** 2940
[12] Diamond P., Itoh S.-I., Itoh K. and Hahm T. 2005 Topical review: zonal flows in plasma–a review *Plasma Phys. Control. Fusion* **47** R35
[13] Chen L., Lin Z. and White R. 2000 Excitation of zonal flow by drift waves in toroidal plasmas *Phys. Plasmas* **7** 3129
[14] Dimits A., Williams T., Byers J. and Cohen B. 1996 Scalings of ion-temperature-gradient-driven anomalous transport in tokamaks *Phys. Rev. Lett.* **77** 71
[15] Dimits A.M. *et al* 2000 Comparisons and physics basis of tokamak transport models and turbulence simulations *Phys. Plasmas* **7** 969
[16] Hinton F. and Rosenbluth M. 1999 Dynamics of axisymmetric and poloidal flows in tokamaks *Plasma Phys. Control. Fusion* **41** A653
[17] Xiao Y., Catto P.J. and Dorland W. 2007 Effects of finite poloidal gyroradius, shaping and collisions on the zonal flow residual *Phys. Plasmas* **14** 055910
[18] Mikkelsen D. and Dorland W. 2008 Dimits shift in realistic gyrokinetic plasma-turbulence simulations *Phys. Rev. Lett.* **101** 135003
[19] Li J. and Kishimoto Y. 2002 Interaction between small-scale zonal flows and large-scale turbulence: A theory for ion transport intermittency in tokamak plasmas *Phys. Rev. Lett.* **89** 115002
[20] Wagner F. *et al* 1982 Regime of improved confinement and high beta in neutral-beam-heated divertor discharges of the asdex tokamak *Phys. Rev. Lett.* **49** 1408
[21] Rogers B., Dorland W. and Kotschenreuther M. 2000 Generation and stability of zonal flows in ion-temperature-gradient mode turbulence *Phys. Rev. Lett.* **85** 5336
[22] Zhu H., Zhou Y. and Dodin I. 2020 Theory of the tertiary instability and the dimits shift from reduced drift-wave models *Phys. Rev. Lett.* **124** 055002
[23] Deng W. and Lin Z. 2009 Properties of microturbulence in toroidal plasmas with reversed magnetic shear *Phys. Plasmas* **16** 102503
[24] Garbet X., Bourdelle C., Hoang G., Maget P., Benkadda S., Beyer P., Figarella C., Voitsekovitch I., Agullo O. and Bian N. 2001 Global simulations of ion turbulence with magnetic shear reversal *Phys. Plasmas* **8** 2793
[25] Levinton F. *et al* 1995 Improved confinement with reversed magnetic shear in tftr *Phys. Rev. Lett.* **75** 4417
[26] Hahm T.S. 1988 Nonlinear gyrokinetic equations for tokamak microturbulence *Technical Report* (Princeton Plasma Physics Lab.(PPPL))
[27] Lee W. 1983 Gyrokinetic approach in particle simulation *Phys. Fluids* **26** 556
[28] Garbet X., Idomura Y., Villard L. and Watanabe T. 2010 Gyrokinetic simulations of turbulent transport *Nucl. Fusion* **50** 043002
[29] Wan Y. *et al* 2017 Overview of the present progress and activities on the cfetr *Nucl. Fusion* **57** 102009
[30] Zhuang G. *et al* 2019 Progress of the cfetr design *Nucl. Fusion* **59** 112010
[31] Duan Y., Xiao Y. and Lin Z. 2022 Gyro-average method for global gyrokinetic particle simulation in realistic tokamak geometry *Plasma Phys. Control. Fusion* **64** 045018
[32] Lee W. 1987 Gyrokinetic particle simulation model *J. Comput. Phys.* **72** 243
[33] Qi L., Kwon J., Hahm T. and Jo G. 2016 Gyrokinetic simulations of electrostatic microinstabilities with bounce-averaged kinetic electrons for shaped tokamak plasmas *Phys. Plasmas* **23** 062513
[34] Angelino P. *et al* 2009 Role of plasma elongation on turbulent transport in magnetically confined plasmas *Phys. Rev. Lett.* **102** 195002
[35] Rewoldt G., Lin Z. and Idomura Y. 2007 Linear comparison of gyrokinetic codes with trapped electrons *Comput. Phys. Commun.* **177** 775
[36] Guo Z., Chen L. and Zonca F. 2009 Radial spreading of drift-wave–zonal-flow turbulence via soliton formation *Phys. Rev. Lett.* **103** 055002
[37] Hahm T., Diamond P., Lin Z., Rewoldt G., Gurcan O. and Ethier S. 2005 On the dynamics of edge-core coupling *Phys. Plasmas* **12** 090903

[38] Merlo G., Dominski J., Bhattacharjee A., Chang C.S., Jenko F., Ku S., Lanti E. and Parker S. 2018 Cross-verification of the global gyrokinetic codes GENE and XGC *Phys. Plasmas* **25** 062308

[39] Chen L., Lin Z., White R. and Zonca F. 2001 Non-linear zonal dynamics of drift and drift-alfvén turbulence in tokamak plasmas *Nucl. Fusion* **41** 747

[40] Yong X. and Catto P.J. 2006 Short wavelength effects on the collisionless neoclassical polarization and residual zonal flow level *Phys. Plasmas* **13** 102311

[41] Yagi M., Ueda T., Itoh S., Azumi M., Itoh K., Diamond P. and Hahm T. 2006 Turbulence spreading in reversed shear plasmas *Plasma Phys. Control. Fusion* **48** A409